Available online at www.sciencedirect.com
SCIENCE DIRECT®
Journal of the European Ceramic Society 25 (2005) 613–626
www.elsevier.com/locate/jeurceramsoc

Diphasic aluminosilicate gels with two stage mullitization in temperature range of 1200–1300 °C

Emilija Tkalcec*, Stanislav Kurajica, Hrvoje Ivankovic

Faculty of Chemical Engineering and Technology, University of Zagreb, Marulićev trg 20, HR-10000 Zagreb, Croatia

Received 6 December 2003; accepted 1 February 2004
Available online 15 June 2004

Abstract

The crystallization of mullite in amorphous diphasic gel aged for 6 months has been studied using non-isothermal differential scanning calorimetry (DSC) and powder X-ray diffraction with Rietveld structure refinement analysis. The diphasic premullite gels undergo structural changes by aging even when they are calcined at 700 °C. These changes imply segregation of the sample to Al_2O_3-rich and SiO_2-rich regions. From the Al_2O_3-rich region crystallizes poorly defined Al–Si spinel at 977 °C followed by two-step mullite crystallization in the temperature interval of 1200–1300 °C. Two overlapped exothermic peaks on DSC scan of aged gel were observed; the first at 1233 °C and the second at 1261 °C. The former is attributed to mullite crystallization by transformation of Al–Si spinel, by which excess alumina occurs, which in the second step of mullitization reacts with amorphous SiO_2-rich phase. The activation energy for mullite crystallization in the first step was $E_a = 935 \pm 14\,kJ\,mol^{-1}$ and the Avrami exponent $n = 2.5$. The values $E_a = 1119 \pm 25\,kJ\,mol^{-1}$ and $n = 1.2$ were obtained for mullite formation in the second step. If amorphous SiO_2-rich phase is extracted from the sample, the value $E_a = 805 \pm 26\,kJ\,mol^{-1}$ is obtained. Mullite crystallizing from Al–Si spinel (when SiO_2-rich phase has been extracted) differentiates compositionally from that formed by both reactions. Smaller unit cell parameters and higher amount of oxygen vacancies are incorporated into tetrahedral positions of mullite structure, as was determined by Rietveld structure refinement method.

Keywords: Mullite; X-ray diffraction; Rietveld structure refinement; Phase development; Kinetics; Gels

1. Introduction

Mullite, $[Al_2^{VI}(Al_{2+2X}^{IV}Si_{2-2X})O_{10-X}$, where $0.17 \leq X \leq 0.58]$ has many favorable characteristics that make it an excellent prospect for engineering applications.[1] High purity and ultra fine mullite powders are important raw materials for optical, structural and electronics applications.[2] Extensive work has been done related to the processing and characterization of sol–gel derived materials having mullite composition. A complete understanding of crystallization behavior and kinetics has not yet been fully achieved.

Premullite gels obtained by sol–gel procedure could be classified according to system homogeneity into two types.[3] Monophasic gels, with molecular homogeneity and direct mullite crystallization from an amorphous phase at ∼980 °C, and diphasic gels, with nanometer level homogeneity, characterized with spinel phase crystallization at ∼980 °C and mullite formation at temperatures higher than 1150 °C. The DTA curve of such diphasic gel is characterized by a strong exotherm at ∼980 °C and a weaker exotherm above 1150 °C. There is limited number of papers, which reported that mullite formation in diphasic gels proceeded by two exothermic events in high temperature interval (1200–1300 °C). The appearance of two exotherms on DTA scans attributed to mullite formation has been described by Chakraborty.[4,5] He proposed that two mullitization reactions proceed by two independent reaction pathways. The first exotherm at ∼1150 °C the author explained as being due to the formation of mullite from SiO_2-rich amorphous phase, while the second one at ∼1250 °C was explained as a consequence of spinel to mullite polymorphic transformation. Hsi et al.[6] also observed two exotherms: the first at 1250 °C and the second at 1300 °C. However, they proposed the former to be the transformation of spinel to mullite, and the latter mullite formation due to the reaction of transient alumina (δ-Al_2O_3 and θ-Al_2O_3) and amorphous SiO_2.

The spinel phase that appears after the exothermic peak at 980 °C has poorly defined X-ray diffraction pattern, which

* Corresponding author.
E-mail address: etkalcec@pierre.fkit.hr (E. Tkalcec).

0955-2219/$ – see front matter © 2004 Published by Elsevier Ltd.
doi:10.1016/j.jeurceramsoc.2004.02.015

exhibits broad peaks very similar to those of γ-Al_2O_3. Therefore, it is difficult to distinguish γ-Al_2O_3 from Al–Si spinel (a solid solution between γ-Al_2O_3 and silica). Despite the intensive investigations the spinel phase is not yet unanimously characterized. The basic disagreement is about the composition of the spinel phase. Some authors consider it as pure γ-Al_2O_3,[7–10] but majority agrees that certain amount of SiO_2 enters the spinel structure. Owing to spinel-type structure the phase was called as Al–Si spinel. The discrepancy about the exact quantity of SiO_2 in Al–Si spinel also arises. Okada and Otsuka[11] proposed phase composition to be $6Al_2O_3{\cdot}SiO_2$. Jin et al.[12] also proposed similar result. Schneider et al.[13] showed that spinel phase might contain up to 18 mol% of SiO_2 incorporated in γ-Al_2O_3. Low and McPherson[14] indicated that spinel composition might be close to that of 2:1 mullite, i.e., $2Al_2O_3{\cdot}SiO_2$, and Chakraborty[15] proposed the composition equal to stoichiometric 3:2 mullite, i.e., $3Al_2O_3{\cdot}2SiO_2$. Srikrishna et al.[16] confirmed that spinel is an aluminosilicate phase and determined its chemical composition to be close to 3:2 mullite.

Many authors using various methods and various precursors have examined mullite crystallization kinetics too. Except for the monophasic gels reported by Li and Thomson[17] and kaolinites,[18] the reported E_a values are in the range of 800–1300 kJ mol^{-1} for various precursor types such as diphasic gels,[12,19–24] hybrid gels,[25] glass fibers[26] and glasses.[27,28] For the single-phase gels reported values are about twice as smaller as for the former groups. Exception is the paper reported by Tkalcec et al.,[29] who obtained the value $E_a = 1053$ kJ mol^{-1} for single-phase gel too. This value is similar to the data for diphasic and hybrid gels, as well as for glasses and glass fibers.

The data concerning the activation energy of Al–Si spinel crystallization are missing in literature. According to Simpson et al.,[30] the activation energy for transformation of amorphous alumina to pure γ-Al_2O_3 is 435 kJ mol^{-1}, and for γ to α transformation 502 kJ mol^{-1}. For the latter, Steiner[31] reported 482 kJ mol^{-1}. Okada et al.[22] reported the value 1092 ± 42 kJ mol^{-1} for the activation energy of simultaneous crystallization of mullite and γ-Al_2O_3. (Al_2O_3/SiO_2 ratio of gel was 80:20).

The aim of this work was to provide information about mullite evolution in diphasic sol–gel derived amorphous premullite powders having DTA curve characterized with two distinct exotherms in temperature interval between 1200 and 1300 °C. The activation energies for mullitization were investigated using Kissinger equation to elucidate the crystallization mechanism attributed to each of these two exothermic events.

2. Experimental

The flow chart of investigation is shown in Fig. 1. The premullite gel was prepared by dissolving $Al(NO_3)_3{\cdot}9H_2O$ (analytical reagent, Kemika) in H_2O, the nitrate/water molar ratio was 1:28. The solution was stirred and refluxed at 60 °C for 1 day. Tetraethoxysilane, (98% purity, Merck) previously mixed with ethanol (TEOS/ethanol molar ratio 1:15) and stirred at room temperature for 1 h, was added dropwise to the nitrate solution. The mixture was stirred under reflux conditions at 60 °C for 8 days. Gel was dried at 105 °C for 3 days, subsequently calcined at 700 °C for 2 h to decompose the organics and remove the volatiles, milled to particles smaller than 63 μm and stored in a desiccator. So prepared calcined powder was immediately performed to DSC analysis. The DSC analysis was repeated after the powder was aged for 6 months in a desiccator. The aged powder was heat-treated at 1000 °C for 2 h, by which Al–Si spinel was formed. This sample is denoted as non-leached (NL) sample. A part of this non-leached powder was treated with 1 M boiling NaOH for 30 min, subsequently filtered, washed with distilled water, dried and re-heated to remove moisture. For convenience, this powder was denoted as leached sample (L). All four samples (calcined, aged, non-leached and leached sample) were characterized by differential scanning calorimetry (DSC). Thermoanalyser NETZSCH 409 with Pt crucibles and corundum as a standard was used.

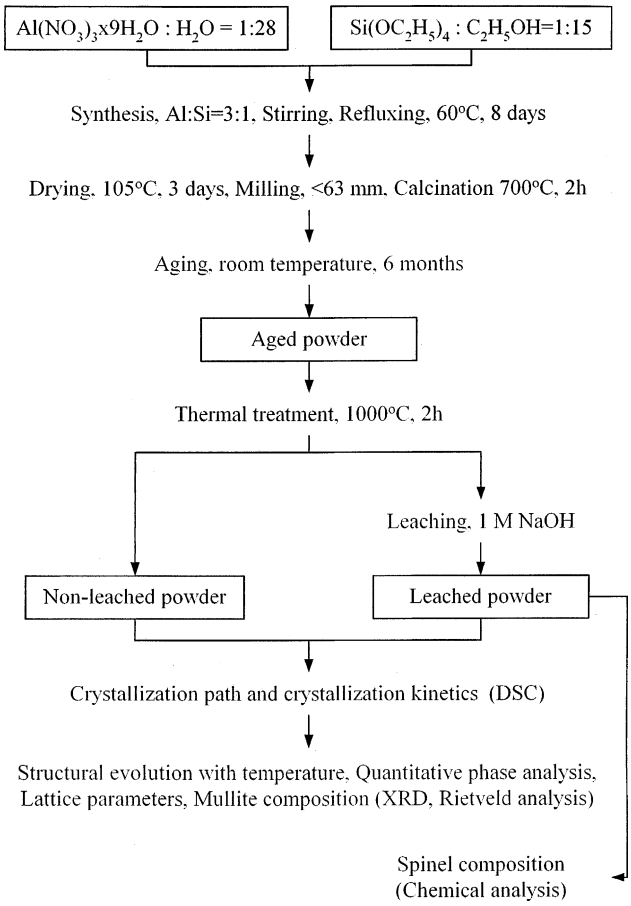

Fig. 1. Flow chart of powder synthesis.

To establish the path of mullite crystallization, the powders were heated to different temperatures and studied by

X-ray diffraction analysis (XRD). Computer controlled diffractometer SIEMENS D 500/PSC using Cu Kα radiation, with quartz single crystal monochromator and a curved position sensitive detector was used. Data were collected between 5 and 70° (2θ) in a step scan mode with step of 0.02° and counting time of 3 s. For the purpose of the Rietveld structure refinement of mullite,[32] the change of its amount and the lattice parameters with temperature, the XRD data were collected using a Philips X'Pert diffractometer with Cu Kα radiation. The peak positions and integral intensities

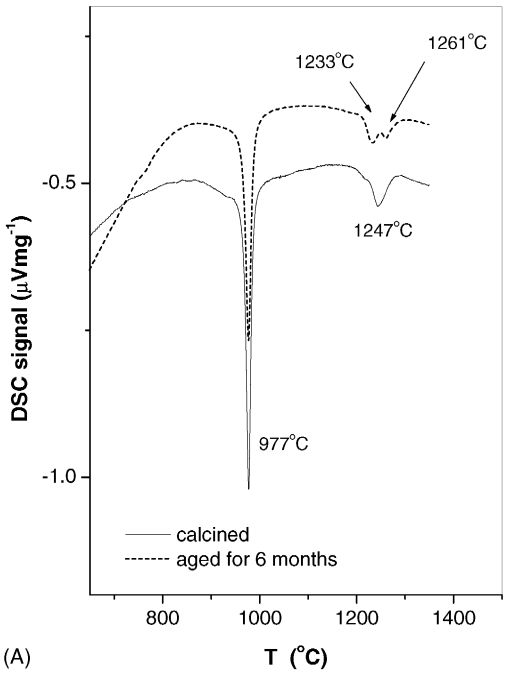

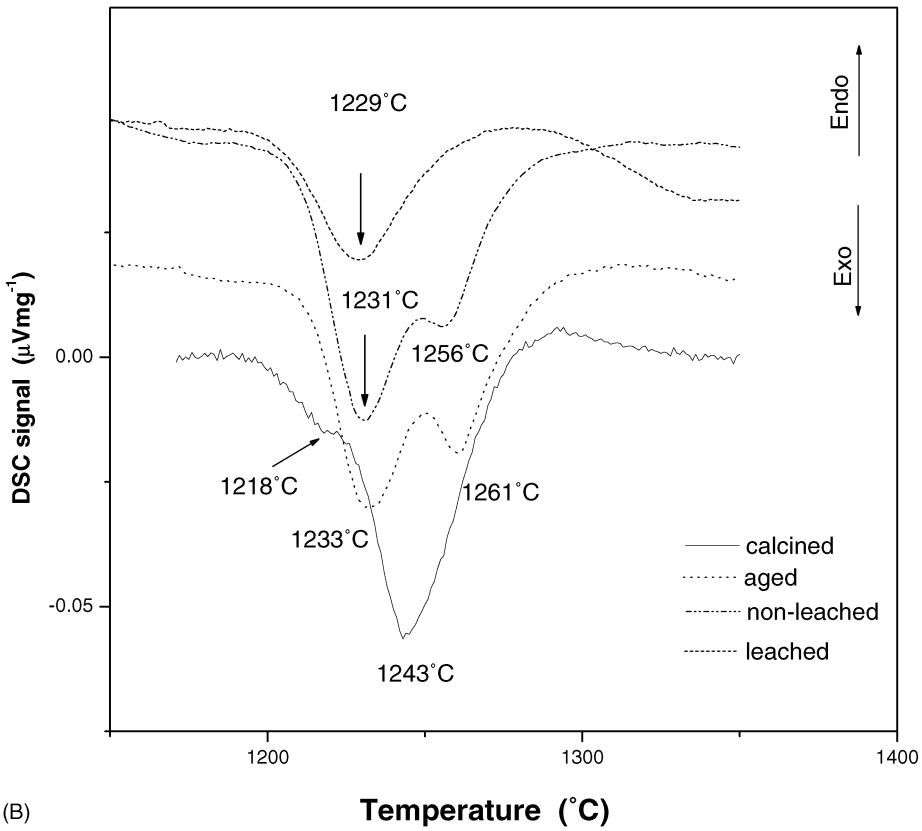

Fig. 2. DSC scans of: (A) calcined and aged samples. (B) calcined, aged, non-leached and leached samples in temperature range of 1100 and 1350 °C.

were collected by step-scanning mode in the range from 15 to 120° with a step size of 0.02° (2θ) and a counting time of 30 s per step. The refinement of mullite structure was started using the parameters reported by Ban and Okada[33] and TOPAS2[34] program. The pseudo Voigt function was used for the modeling of diffraction profiles. In the final refinements the following parameters were refined: scale factor, 2θ zero, seven coefficients of Chebyshev polynomial to describe the background, peak profile parameters, unit cell parameters determined using Si as a standard, *x*, *y*, *z* atom positions, occupation factors and isotropic temperature factors. The change of unit cell parameters with temperature was evaluated on the samples containing Si as a standard. The amount of alumina in mullite structure was calculated using the Ban and Okada relation:[33]

$$Al_2O_3\ (\text{mol\%}) = 1433 \times (\text{length of } a\text{-axis}) - 1028.06 \quad (1)$$

The activation energies for nucleation and growth of Al–Si spinel (in aged gel) and mullite in NL (non-leached) and L (leached) samples were evaluated from the exothermic DSC peaks at 977 °C, and the exothermic peaks in the range of 1200–1300 °C, using Kissinger equation[35] as follows:

$$\ln\frac{\beta}{T_p^2} = -\frac{E_a}{RT_p} + C \quad (2)$$

where β is the heating rate, T_p is the exothermic peak temperature, E_a is the activation energy for nucleation and growth, R is the universal gas constant and C is a constant. According to Augis and Bennet,[36] the crystallization mechanism can be determined from the Avrami exponent, n, of the exothermic peak represented by:

$$n = \frac{2.5T_p^2 R}{\Delta T E_a} \quad (3)$$

where ΔT is full width at half maximum of exothermic peak (FWHM). However, this method is not applicable for overlapped peaks, therefore, to determine the Avrami exponent n for each of the two overlapped peaks of NL sample, the separation of the peaks was made using computer resolving method,[37] which enables simultaneous evaluation of the sum of activation energy and Avrami exponent ($E_a \times n$). Knowing the activation energy from the Kissinger plot, the Avrami exponent could be then calculated.

3. Results

DSC scans of calcined and aged powders are given in Fig. 2A. The DSC scan of calcined powder (700 °C for 2 h) is characterized by a dominant exotherm at 977 °C, and a much smaller peak at 1247 °C with a shoulder on the left side of the peak. On DSC scan of aged sample, in addition to the peak at 977 °C, two partially resolved peaks in high temperature range were observed; the first at 1233 °C and the second at 1261 °C. DSC scans of all four samples

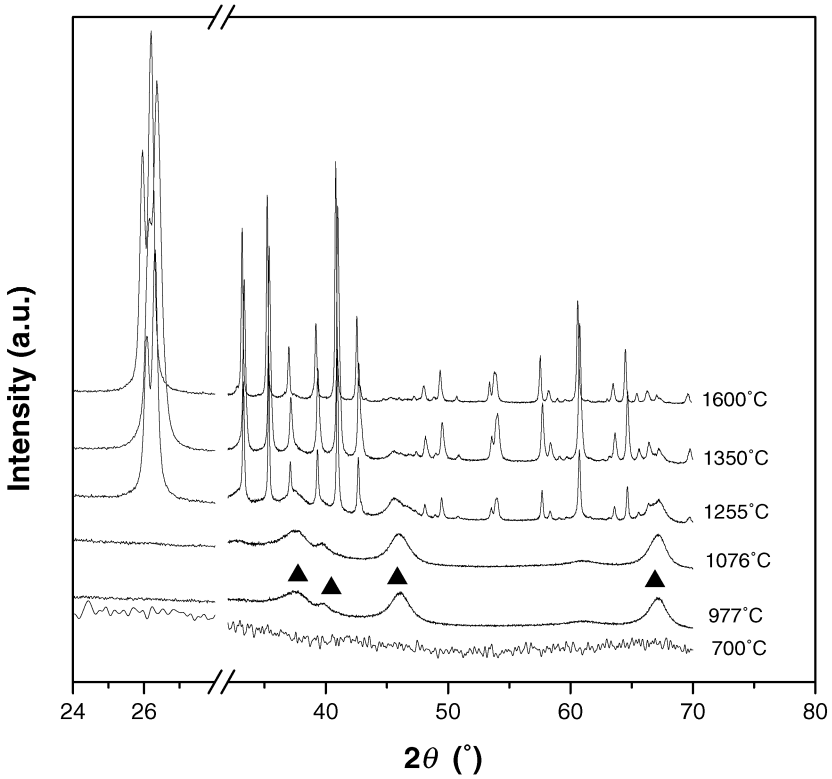

Fig. 3. XRD patterns of the aged gel heat treated to a various temperatures. (▲) Al–Si spinel. Mullite lines are not marked.

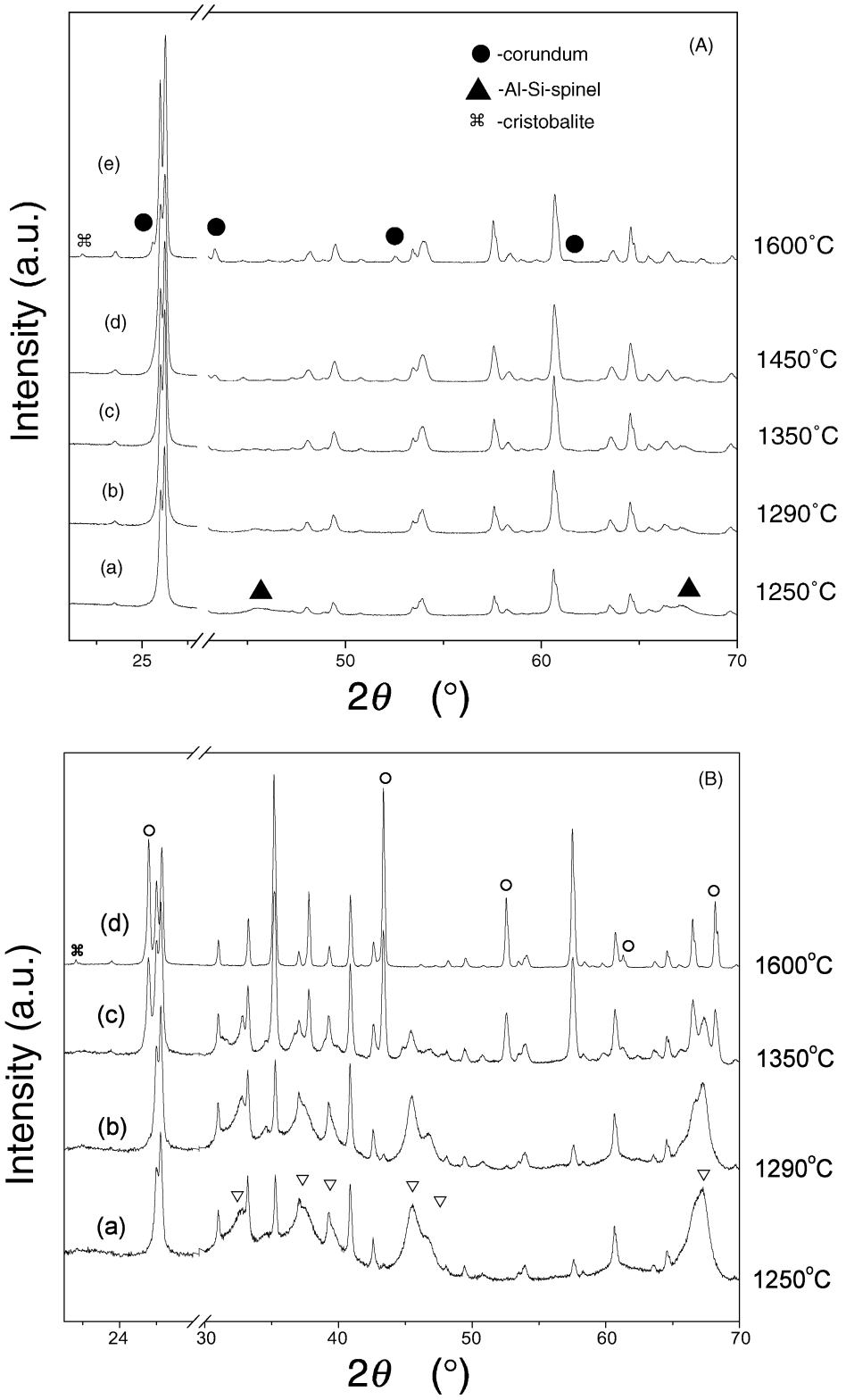

Fig. 4. XRD patterns of: (A) non-leached and (B) leached samples heat-treated to various temperatures: (a) 1250 °C; (b) 1290 °C; (c) 1350 °C; (d) 1450 °C; (e) 1600 °C. (▲) Al-Si spinel in non-leached sample; (●) corundum in non-leached sample; (▽) transient alumina (δ-Al_2O_3 and θ-Al_2O_3) in leached sample; (○) corundum in leached sample; (⌘) cristobalite. Only non-overlapped lines of corundum are marked. Mullite lines are not marked.

(calcined, aged, non-leached and leached samples) in temperature range of 1100–1350 °C are given in Fig. 2B. With the sample heat treated at 1000 °C for 2 h (NL sample) the peak at 977 °C is, of course, missing and the peak at 1233 °C becomes somewhat greater and shifted to 1231 °C. Simultaneously, the peak at 1261 °C is shifted to 1256 °C. The DSC scan of L sample in temperature range of 1200–1300 °C exhibited only one exothermic peak at 1229 °C. That means that the component related to the second exothermic peak is extracted by the leaching. To confirm the identity of the exothermic events, DSC analyses of aged gel, non-leached (NL) and leached (L) powders were stopped at different temperatures and the samples were quenched and performed to XRD analysis. XRD patterns are shown in Figs. 3 and 4. The analyses reveal that the aged powder (Fig. 3) is amorphous up to the first exotherm on DSC scan at 977 °C, after this point the XRD pattern displays only weakly crystallized Al–Si spinel, which transforms into orthorhombic mullite between 1200 and 1300 °C. There is still somewhat spinel phase at 1350 °C, but at 1600 °C mullite is the sole phase determined. The comparison of XRD patterns of the aged gel (Fig. 3) and NL sample (Fig. 4A) shows that there is a difference in phase analyses only at 1600 °C. In the aged gel mullite is the sole phase determined, whereas in the NL powder small amount of corundum (α-Al_2O_3) and traces of cristobalite were also observed. The XRD pattern of L sample heated up to 1250 °C (Fig. 4B) shows much smaller amount of mullite than that of NL sample at the same temperature, and γ-Al_2O_3 is already transformed into δ- and θ-Al_2O_3, which further transforms into corundum above 1300 °C. Traces of cristobalite are observed in L sample heat-treated at 1600 °C.

The lattice parameters of mullite in NL and L samples containing Si as a standard were compared and the data are shown in Fig. 5. The *a*- and *c*-axes of mullite in both samples decrease with temperature and the *b*-axes show the tendency to increase in a small extent. That is in accordance to literature. However, the unit cell of mullite in L sample is evidently smaller than in the NL sample in the whole temperature interval studied. The amount of alumina in mullite structure calculated by using Eq. (1) is shown in Fig. 6. Mullite at 1250 °C in the NL sample contains 65.7 mol% Al_2O_3, and with the temperature increase it decreases approaching to the value of stoichiometrical 3:2 mullite, but even at 1600 °C its composition does not fit the theoretical value for 3.2 mullite. Mullite in L sample at 1250 °C contains smaller amount of Al_2O_3 (64.4 mol%), which also decreases with temperature, at the beginning faster and above 1350 °C slower. Thus, it also does not reach the stoichiometric 3:2 composition up to 1600 °C.

In order to determine structure parameters of individual phases (primarily the incorporation of alumina in tetrahedral position in mullite structure) and the change of mullite amount with heat-treated temperature, we fitted the experimental powder diffraction patterns with the profile fitting functions based on known crystal structure information[33]

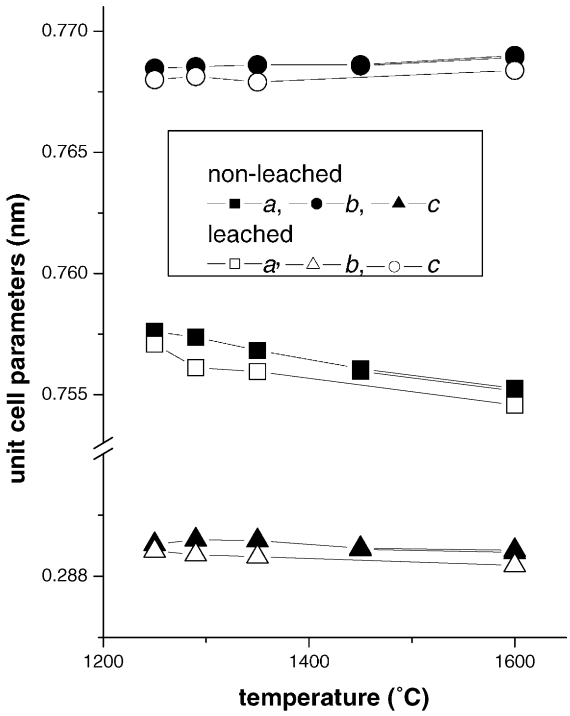

Fig. 5. Unit cell parameters of non-leached and leached samples as a function of firing temperature. Standard deviations are smaller than the height of the marks.

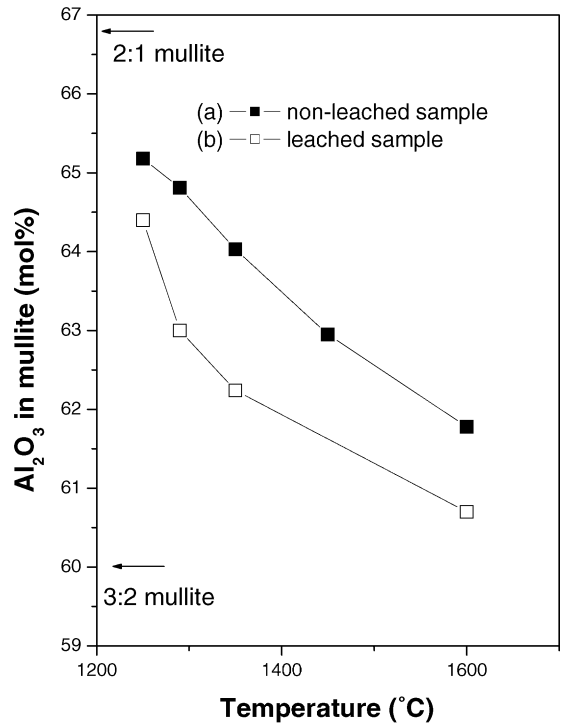

Fig. 6. Alumina content in mullite at different temperatures of (■) non-leached and (□) leached sample determined by Ban and Okada relation (1). Lines are introduced as guides for the eye.

Table 1
Wykoff sites, atomic fractional coordinates, the "names" of atom positions and occupancies in the average mullite structure given by Ref. 33 space group *Pbam* (No. 55)

Atoms	Al	Si, Al	Al	O	O	O	O
Wykoff sites	2a	4h	4h	4h	4g	2d	4h
Coordinates	0, 0, 0	*x*, *y*, 1/2	*x*, *y*, 1/2	*x*, *y*, 1/2	*x*, *y*, 0	0.5, 0, 0.5	*x*, *y*, 0.5
"Names" of atom positions	Al(1)	T	Al(2)	O(1)	O(2)	O(3)	O(4)
Occupancies	1	Al 0.5, Si (0.5 − *X*)	*X*	1	1	1 − 3*X*	*X*

by Rietveld structure refinement method.[32] Mullite the solid solution of Al_2O_3 and SiO_2 may be represented by general formula: $Al_2^{VI}(Al^{IV}_{2+2X}Si_{2-2X})O_{10-X}$ where Al in excess of 4 replaces Si atom in 4 h site (Table 1) resulting in an oxygen vacancy at the tetrahedral corner sharing position O(3). This leads to a local structural rearrangement shifting the excess Al atom on to a new position Al(2) and the corresponding next neighbor oxygen on to the shifted position O(4). The difference between various mullites structurally manifest itself by variations of the cell dimensions; and essentially by variations of the positions and occupancies at Al(2) and O(4) positions. The unit cell parameters, Wykoff sites, the occupancy and the "names" of the atom positions in the structure are given in Table 1. As shown from Table 1, there are 10 positional parameters in mullite structure, but the occupancy parameter necessary for determination in the structure refinement was only the parameter *X*. All other occupancies have been given constraints to this parameter.

Table 2
Structural parameters of mullite in NL sample at different heat-treatment temperature

	Temperature (°C)				
	1250	1290	1350	1450	1600
a (nm)	0.75757(3)	0.75741(2)	0.75682(2)	0.75599(2)	0.75532(2)
b (nm)	0.76846(3)	0.76856(2)	0.76848(2)	0.76861(3)	0.76892(2)
c (nm)	0.288523(9)	0.288582(7)	0.288523(7)	0.288420(8)	0.288404(6)
x (Al 1)	0	0	0	0	0
y (Al 1)	0	0	0	0	0
z (Al 1)	0	0	0	0	0
Occ.(Al 1)	1	1	1	1	1
x (T)	0.15085(4)	0.15103(2)	0.1508(2)	0.1502(2)	0.1501(2)
y (T)	0.34315(4)	0.34150(2)	0.3414(2)	0.3414(3)	0.3413(2)
z (T)	1/2	1/2	1/2	1/2	1/2
Occ.(Al)	0.5	0.5	0.5	0.5	0.5
Occ.(Si)	0.337	0.353	0.3344	0.334	0.363
x (Al 2)	0.267(2)	0.264(1)	0.267(1)	0.267(1)	0.262(1)
y (Al 2)	0.216(2)	0.210(1)	0.214(1)	0.216(1)	0.216(1)
z (Al 2)	1/2	1/2	1/2	1/2	1/2
Occ.(Al 2)	0.162	0.147	0.156	0.156	0.139
x (O1)	0.3542(7)	0.3501(4)	0.3570(4)	0.3543(4)	0.3545(3)
y (O1)	0.4281(4)	0.4256(3)	0.4244(3)	0.4235(4)	0.4237(3)
z (O1)	1/2	1/2	1/2	1/2	1/2
Occ.(O1)	1	1	1	1	1
x O(2)	0.1312(7)	0.1289(3)	0.1271(4)	0.1274(4)	0.1268(3)
y (O2)	0.2215(4)	0.2212(2)	0.2203(3)	0.2232(3)	0.2218(3)
z (O2)	0	0	0	0	0
Occ.(O2)	1	1	1	1	1
x O(3)	1/2	1/2	1/2	1/2	1/2
y O(3)	0	0	0	0	0
z (O3)	1/2	1/2	1/2	1/2	1/2
Occ.(O3)	0.512	0.559	0.533	0.533	0.583
x O(4)	0.421(3)	0.429(2)	0.436(2)	0.445(2)	0.442(3)
y (O4)	0.079(4)	0.072(2)	0.071(3)	0.055(3)	0.062(3)
z (O4)	1/2	1/2	1/2	1/2	1/2
Occ.(O4)	0.162	0.147	0.156	0.156	0.139
R_{wp}	0.0945	0.0688	0.0932	0.1043	0.0900
R_{Bragg}	0.1222	0.0727	0.0744	0.0675	0.065
Temperature factor	2.14	1.91	1.10	1.20	1.55

Numbers in parentheses correspond to std. for last place quoted.

Table 3
Structural parameters of mullite in L sample at different heat-treatment temperature

	Temperature (°C)			
	1250	1290	1350	1600
a (nm)	0.75708(6)	0.75616(6)	0.75590(4)	0.75457(2)
b (nm)	0.76875(5)	0.76830(5)	0.76797(4)	0.76840(2)
c (nm)	0.28841(2)	0.28801(2)	0.288315(1)	0.288174(7)
x (Al 1)	0	0	0	0
y (Al 1)	0	0	0	0
z (Al 1)	0	0	0	0
Occ.(Al 1)	1	1	1	1
x (T)	0.1545(10)	0.1591(9)	0.1522(7)	0.1493(4)
y (T)	0.3401(9)	0.3368(9)	0.3401(7)	0.3418(4)
z (T)	1/2	1/2	1/2	1/2
Occ.(Al)	0.5	0.5	0.5	0.5
Occ.(Si)	0.333	0.350	0.354	0.363
x (Al 2)	0.263(4)	0.2629(4)	0.240(4)	0.2449(1)
y (Al 2)	0.213(4)	0.219(4)	0.245(4)	0.216(1)
z (Al 2)	1/2	1/2	1/2	1/2
Occ.(Al 2)	0.167	0.150	0.145	0.139
x (O1)	0.3479(15)	0.3505(10)	0.3523(9)	0.3577(5)
y (O1)	0.4233(10)	0.4290(10)	0.4250(9)	0.4251(5)
z (O1)	1/2	1/2	1/2	1/2
Occ.(O1)	1	1	1	1
x O(2)	0.1508(15)	0.1073(10)	0.1206(9)	0.1262(5)
y (O2)	0.2207(8)	0.2157(8)	0.2178(7)	0.2205(4)
z (O2)	0	0	0	0
Occ.(O2)	1	1	1	1
x O(3)	1/2	1/2	1/2	1/2
y O(3)	0	0	0	0
z (O3)	1/2	1/2	1/2	1/2
Occ.(O3)	0.499	0.550	0.565	0.591
x O(4)	0.487(9)	0.528(9)	0.439(6)	0.442(3)
y (O4)	0.086(9)	0.096(9)	0.070(8)	0.062(3)
z (O4)	1/2	1/2	1/2	1/2
Occ.(O4)	0.167	0.150	0.145	0.136
R_{wp}	0.0945	0.0623	0.0794	0.0687
R_{Bragg}	0.0154	0.021	0.0444	0.0383
Temperature factor	2.4(2)	1.2(2)	1.0(3)	2.6(1)

Numbers in parentheses correspond to std. for last place quoted.

Table 2 summarizes the data obtained by Rietveld structure refinements for NL sample heat treated at different temperatures, and Table 3 the refinements data for L sample. The changes of occupancies in Al(2) position with heat-treatment temperature in the samples NL and L are shown in Fig. 8.

Quantitative phase analyses performed on L sample heat-treated at 1250, 1290, 1350 and 1600 °C, and on NL sample heat-treated at 1450 and 1600 °C, i.e., on the specimens where amorphous phase could be neglected and those containing no Al–Si spinel, are given in Fig. 7 and Table 4. (For other specimens obtained by heat-treatment of NL sample the analyses are not realistic, since by structure refinement the amount of amorphous phase, as well as Al–Si spinel is not taken into consideration.)

To determine the chemical composition of spinel and amorphous phase, aged sample was first thermally treated at 1000 °C for 2 h to promote spinel crystallization and afterwards treated with boiling 1 M NaOH to extract the amorphous phase out of the sample. The composition of both components: solid (denoted as leached sample) and liquid (extracted amorphous phase) were determined by wet chemical analyses. It was found that leached sample contains 21 mol% SiO_2, which is incorporated in the structure of γ-Al_2O_3, and the composition of the extracted phase was: 76 mol% SiO_2 and 24 mol% Al_2O_3.

Crystallization kinetics was conducted to provide some additional information regarding the mechanisms of mullite formation in two steps. The Kissinger plots of $\ln(\beta/T_p^2)$ versus $1/T_p$[35] for exothermic peaks at 1231 and 1256 °C of NL sample and for the peak at 1229 °C of the L sample attributed to mullite formation are presented in Fig. 9. The plot for the peak at 977 °C observed on aged sample and attributed to spinel formation is also shown in this figure. The activation energies were calculated from the slopes of the linear fits to the experimental data using Eq. (2) and presented in Table 5. To calculate the Avrami exponent for each of the two overlapped peaks in non-leached sample, the peaks were first

Table 4
Quantitative phase analysis of non-leached and leached sample obtained by Rietveld refinement

Sample	Temperature (°C)	Phase analysis (wt.%)			
		Mullite	α-Al_2O_3	Al–Si spinel or γ-Al_2O_3	Transient alumina (δ- and θ-Al_2O_3)
Non-leached	1250[a]	+	–	+	–
	1290[a]	+	–	+	–
	1350[a]	+	–	+	–
	1450	97.5	2.5	–	–
	1600[b]	94.0	6.0	–	–
Leached at 1000 °C[c]	1250	13.3	–	–	86.7 (72.3 + 14.4)
	1290	14.2	–	–	85.8 (58.9 + 26.9)
	1350	32.7	27.2	–	40.1 (0 + 40.1)
	1600	46.1	53.9	–	–

The amount of amorphous phase has not been taken into consideration.

[a] Al–Si spinel is not taken in evaluation by Rietveld refinement, since its structure is unknown. Amorphous phase present in the samples marked by arrows is also not taken into procedure of structural refinement, therefore the obtained sample composition is not real and is not given in the table.

[b] It is assumed that the amount of amorphous (glassy) phase is very small at 1600 °C.

[c] The amorphous phase is leached out by treatment with NaOH.

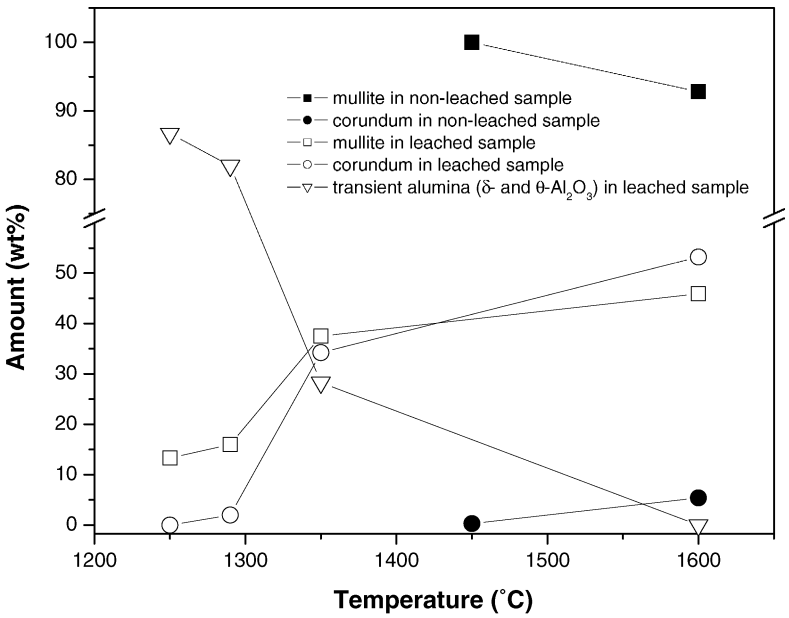

Fig. 7. Quantitative phase analysis of non-leached and leached samples, as a function of temperature. (■) Mullite in non-leached sample; (●) corundum in non-leached sample; (□) mullite in leached sample; (○) corundum in leached sample; (▽) transient alumina (δ-Al_2O_3 and θ-Al_2O_3) in leached sample.

resolved by the method described in our work,[37] and then the Avrami exponent was calculated. TEM micrograph of the non-leached sample heat-treated at 1260 °C is shown in Fig. 10. The possible sequential reactions of mullite formation in two steps are proposed by chart in Fig. 11.

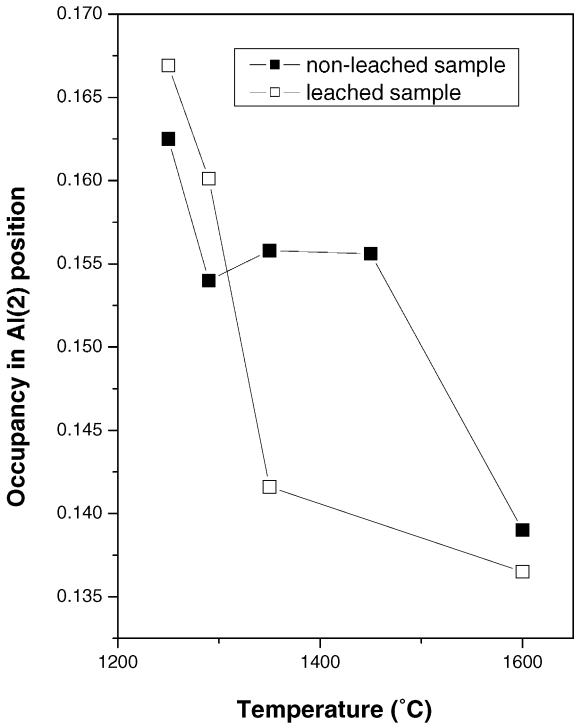

Fig. 8. The occupancy of aluminum in Al(2) position in mullite structure for NL and L sample.

4. Discussion

4.1. DSC analyses and X-ray diffraction of non-leached and leached samples

It is well documented in literature[38–42] that the strong exothermic peak at about 980 °C and smaller one between 1200 and 1300 °C on DSC scans of diphasic gels are due to crystallization of γ-Al_2O_3/or Al–Si spinel and mullite, respectively. However, there is limited number of papers, which reported that mullite crystallization proceeds by two exothermic events in the high temperature interval.[4–6] Chakraborty[4,5] and Hsi et al.[6] agree that two peaks in high temperature region are due to the separation of amorphous gel to Al_2O_3-rich and SiO_2-rich regions. However, their opinions which of the peaks should be attributed to spinel transformation are mismatched. On the other hand, neither Chakraborty nor Hsi et al. gave an explanation under which experimental conditions two high-temperature peaks of mullite crystallization occur. From our results it is clearly seen (Fig. 2A and B) that diphasic gels undergo structural changes by aging even if they are calcined at 700 °C. These changes imply segregation of sample to Al_2O_3-rich and SiO_2-rich regions and mullite crystallizes from each separate region in a somewhat different temperature interval. As a consequence, the exothermic peak on DSC scan between 1200 and 1300 °C splits by aging in two partially overlapped peaks. This segregation is further intensified by heat treatment at 1000 °C for 2 h; therefore a small amount of corundum at 1600 °C determined only in non-leached sample, could be attributed to the presence of pure γ-Al_2O_3 in addition to Al–Si spinel at 980 °C.

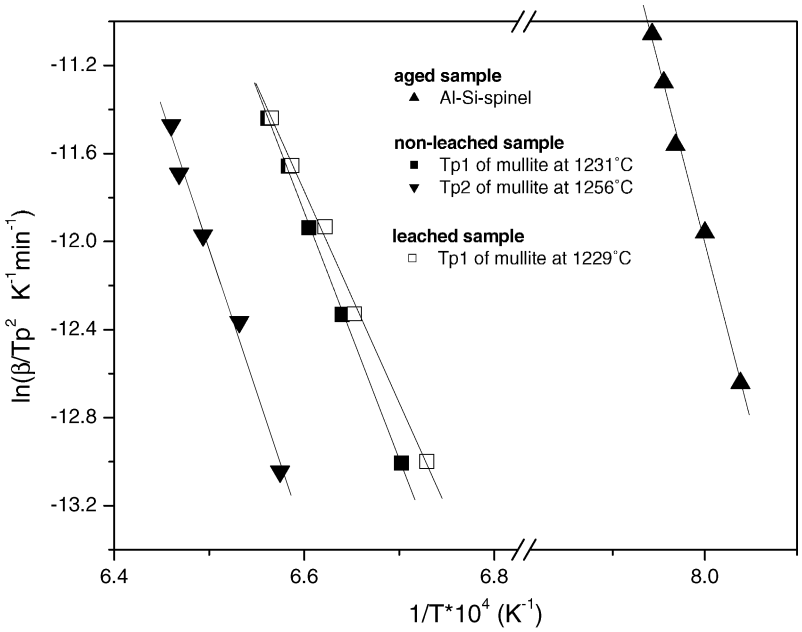

Fig. 9. Kissinger plots of $\ln(\beta/T_p^2)$ vs. $1/T_p$. (▲) Al–Si spinel; (■) mullite peak at 1231 °C; (▼) mullite peak at 1256 °C; (□) mullite peak at 1229 °C in the leached sample.

In order to resolve from which separated region mullite started to crystallize first, we leached out the amorphous SiO_2-rich phase and separately conducted the transformation of Al–Si spinel to mullite. After extraction of an aged gel with NaOH only the first peak on DSC scan remained but shifted from 1233 to 1229 °C. Therefore, the peak at 1233 °C on DSC scan of aged sample (or the peak at 1231 °C on DSC scan of NL sample) could be attributed to mullite formation by transformation of spinel. This transformation is accompanied by the release of excess alumina, which reacts with amorphous SiO_2-rich phase forming mullite. When amorphous SiO_2-rich phase is missing, the excess of alumina is transformed by further heat-treatment in δ-Al_2O_3 and θ-Al_2O_3. Therefore, on XRD pattern of the leached sample at 1250 °C (Fig. 4B) mullite and transient alumina (mixture of δ-Al_2O_3 and θ-Al_2O_3) were determined. Above 1300 °C, the transient alumina transforms into corundum. Accordingly, only one peak on DSC scan of leached sample (Fig. 2B) and formation of corundum above 1300 °C points out the evidence that the first exotherm in temperature range of 1200–1300 °C in the aged and non-leached sample is related to mullite formation from Al–Si spinel.

Under assumption that entire amorphous part of the sample was leached out the composition of spinel was found to contain 21 mol% (14 wt.%) SiO_2. This value is somewhat higher than that obtained by Schneider et al.,[13] who showed that spinel phase may contain up to 18 mol% SiO_2 incorporated in γ-Al_2O_3. However, the authors[13] indicated that the amount of silica in spinel is temperature dependent. Taking into consideration that the as-prepared gel was first calcined at 700 °C and afterwards aged for 6 months and additionally heat treated at 1000 °C for 2 h before the leaching, the higher amount obtained could be understood.

The smaller unit cell parameters of mullite crystallizing in L sample at 1250 °C in comparison to mullite in non-leached sample (Fig. 5) can be attributed to higher occupancies of Al atoms in Al(2) positions (determined by Rietveld structure refinement), and consequently, to greater number of oxygen vacancies in the structure of this mullite (see Fig. 8 and Table 3). Upon further heating the number of oxygen vacancies decreases and is accompanied by a depopulation of Al-atoms at the Al(2) positions in favor of an increase of Si atoms at the "normal" tetrahedral (T) sites. Accordingly, mullite progressively adjusts its composition to a thermodynamically stable 3:2 composition. Simultaneously the dimension of unit cell decreases. The same continuous decrease of oxygen vacancies versus temperature was expected also in NL sample. However, in this sample crystallization

Table 5
Activation energies for mullite and Al–Si spinel crystallization obtained by Kissinger[35] method

	Non-leached sample		Sample leached at 1000 °C	
DSC peak (°C)	977	1231	1256	1229
Crystalline phase	Al–Si spinel	Mullite I	Mullite II	Mullite I
Activation energy (kJ mol^{-1})	1263 ± 53	937 ± 14	1119 ± 25	805 ± 26

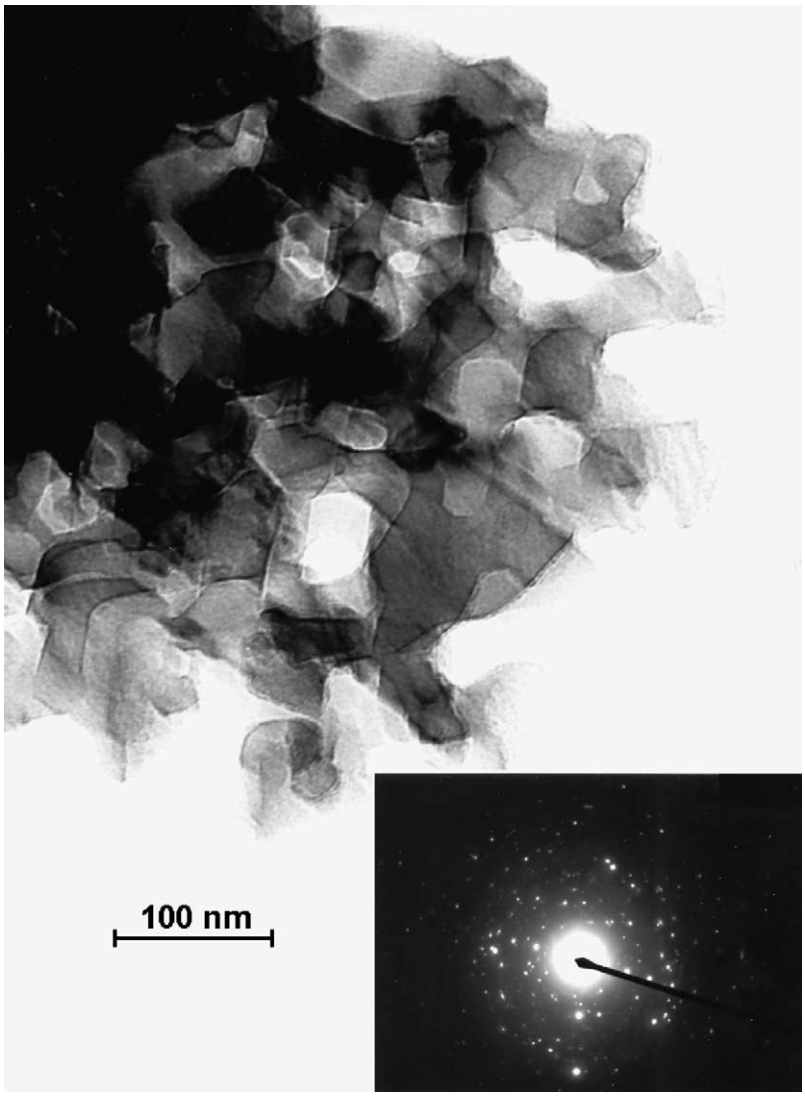

Fig. 10. TEM micrograph and corresponding diffraction pattern of aged sample heat-treated at 1260 °C for 2 h.

of mullite occurs in two steps, and during the second step crystallizes mullite with higher amount of oxygen vacancies, which brings about a discontinuity on the plot of Al(2) occupancy versus temperature in Fig. 8. It is in accordance with results of Johnson et al.[28] who found that mullite with higher alumina content, consequently, with higher Al in Al(2) position and higher O(3) vacancies has smaller lattice energy.

Quantitative phase analyses obtained by Rietveld structure refinement (Fig. 7) for NL sample is realistic only for specimens heat-treated at 1450 and 1600 °C, since they contain no Al–Si spinel and the amount of amorphous (glassy) phase could be neglected. The appearance of corundum at 1450 °C (2.5 wt.%) and 1600 °C (6.0 wt.%) could be understood that the separation can continue to larger area of pure alumina. In L sample heated up to 1250 °C about 13.3 wt.% of mullite and 86.7 wt.% of transient alumina (72.3 wt.% of δ-Al_2O_3 and 14.4 wt.% of θ-Al_2O_3) were determined. Since the amorphous SiO_2-rich phase was extracted in L sample, alumina becomes an excess in the system and transforms itself first in δ- and θ-Al_2O_3 and above 1290 °C into corundum. At 1350 °C, the sample contains 32.7 wt.% of mullite and 27.2 wt.% of corundum, whereas the amount of transient alumina (only θ-Al_2O_3) is reduced to 40.1 wt.%. At 1600 °C, 46.1 wt.% mullite and 53.9 wt.% corundum are determined. Traces of cristobalite are also detected.

The assumed processes, which occur in non-leached sample during the heat-treatment are scheduled in Fig. 11. Segregation of amorphous gel by aging brings about the crystallization of mullite from Al–Si spinel, the composition of which is changing in favor of silica increase in the structure. The second step mullite crystallization (by a reaction of amorphous silica and excess of alumina) brings a temporarily increase of alumina content in average composition of mullite.

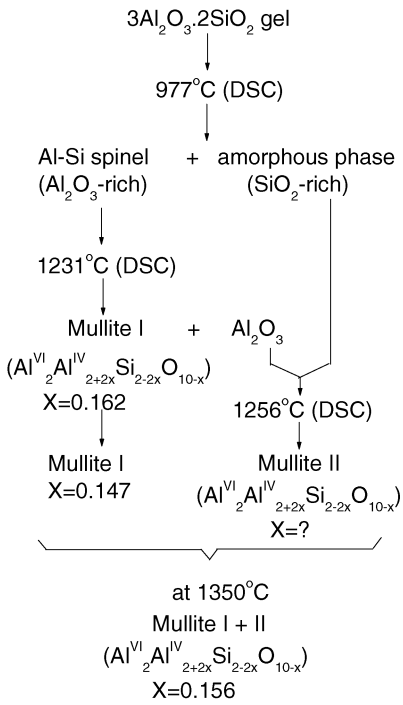

Fig. 11. Proposed sequential reactions occurring during heating of aged powder or non-leached sample.

4.2. Kinetics of spinel and mullite formation

As mentioned above, the data concerning the activation energy of Al–Si spinel crystallization are missing in literature. The kinetic parameters for Al–Si spinel crystallization at 977 °C obtained in this work were: $E_a = 1263 \pm 55\,kJ\,mol^{-1}$ and $n = 2.5$. Okada et al.[22] investigated the kinetics of simultaneous crystallization of mullite and γ-Al_2O_3 from glasses by non-isothermal DTA and obtained the value $E_a = 1092 \pm 42\,kJ\,mol^{-1}$, and the Avrami parameter $n = 2.6$. The authors[22] proposed that mullitization processes in diphasic and hybrid gels, as well as in glasses, glass fibers and in single-phase gels are similar irrespective of their mullitization routes and temperatures. According to Okada et al.[22] all these processes are considered to occur by a similar diffusion-controlled mechanism. According to them the differences in the crystallization temperature arise from differences in the diffusion path length necessary to form mullite.

The obtained activation energy and Avrami exponent (Table 5) for mullite formation from Al–Si spinel (peak at 1231 °C), in the presence of segregated SiO_2-rich phase, were: $E_a = 935 \pm 14\,kJ\,mol^{-1}$ and $n = 2.5$. Somewhat smaller value ($805 \pm 26\,kJ\,mol^{-1}$) is obtained when the amorphous SiO_2-rich phase is extracted. The values $E_a = 1119 \pm 25\,kJ\,mol^{-1}$ and $n = 1.2$ were obtained for mullite formation by reaction of SiO_2-rich phase and alumina, represented by the peak at 1256 °C. According to these results, there exists small difference between the activation energy of mullite formation from segregated Al–Si spinel (peak at 1231 °C) and SiO_2-rich amorphous phase (peak at 1256 °C), however, the Avrami exponents *n* are unmistakable different (2.5 and 1.2, respectively). Accordingly, it seems that in the former process nucleation and three-dimensional growth of mullite grains are operating, as proposed by the most authors, however, in the latter previously formed mullites serve as seeding for mullitization in amorphous SiO_2-rich region. That is in accordance with the microstructure of the same mullite body sintered at 1260 and 1600 °C. Whereas equiaxial mullite grains are characteristic for mullite sintered at 1260 °C (Fig. 10), bimodal distribution of mullite grains (long mullite grains embedded in the smaller equiaxed mullite matrix) are characteristic for sample heated up to 1600 °C (see Fig. 8A in our paper[23]). According to Kanka and Schneider[43] liquid-phase sintering produces the latter microstructure, whereas the former microstructure (equiaxed mullite grains) is a result of a solid-state sintering process. Furthermore, they believe, that the presence of liquid SiO_2-rich phase has a decisive influence on the mode of mullite crystal growth and associated microstructural developments of sample specimens. Therefore, it is reasonable to assume that different microstructures of the same sample sintered at 1260 and 1600 °C could also be the result of different mullite formation mechanism from Al–Si spinel and from amorphous SiO_2-rich phase. The small difference in activation energies of mullite formation from Al–Si spinel and amorphous phase can be caused by differences in diffusion path length necessary to form mullite crystals.

5. Conclusion

(i) The diphasic premullite gels undergo structural changes by aging even when they are calcined at 700 °C. These changes imply segregation of the sample to Al_2O_3-rich and SiO_2-rich regions. From the Al_2O_3-rich region crystallizes poorly defined Al–Si spinel at about 980 °C followed by mullite crystallization at about 1233 °C. From SiO_2-rich amorphous phase mullite crystallizes directly at somewhat higher temperature. As a consequence, the exothermic peak on DSC scan between 1200 and 1300 °C attributed to mullite formation splits in two partially overlapped peaks.

(ii) Mullite crystallizing from Al–Si spinel (when SiO_2-rich phase has been extracted) differentiates also compositionally from that formed by both reactions. Smaller unit cell parameters, and higher amount of oxygen vacancies incorporated into tetrahedral positions of mullite structure were determined by Rietveld structure refinement method.

(iii) The activation energy of mullite formed by transformation of Al–Si spinel is somewhat smaller than the activation energy of mullite crystallizing in amorphous SiO_2-rich phase ($937 \pm 14\,kJ\,mol^{-1}$ and

$1119 \pm 25\,\mathrm{kJ\,mol^{-1}}$, respectively). The Avrami exponents determined for each of the separate phases are: $n = 2.5$ (transformation of Al–Si spinel into mullite) and $n = 1.2$ for mullite formation by reaction of transient alumina with amorphous SiO_2-rich phase. Accordingly, two different mechanisms are operating in mullite crystallization from these two separate phases.

(iv) The kinetic parameters for Al–Si spinel formation at 977 °C are: $E_a = 1263 \pm 55\,\mathrm{kJ\,mol^{-1}}$ and $n = 2.5$.

Acknowledgements

The authors acknowledge the financial support provided by the Ministry of Science and Technology, Republic of Croatia.

References

1. Aksay, I. A., Dabbs, D. M. and Sarikaya, M., Mullite for structural, electronic, and optical applications. *J. Am. Ceram. Soc.* 1991, **74**(10), 2343–2358.
2. Schneider, H., Okada, K. and Pask, J., *Mullite and Mullite Ceramics*. Wiley, Chichester, 1994, p. 186.
3. Sundaresan, S. and Aksay, I. A., Mullitization of diphasic aluminosilicate gels. *J. Am. Ceram. Soc.* 1991, **74**(10), 2388–2392.
4. Chakraborty, A. K., Role of hydrolysis water-alcohol mixture on mullitization of Al_2O_3–SiO_2 monophasic gels. *J. Mater. Sci.* 1994, **29**, 6131–6138.
5. Chakraborty, A. K., DTA characterisation of three types of Al_2O_3–SiO_2 gels made from TEOS–$Al(OBU)_3$ mixture with variation of water. *Ceram. Int.* 1996, **22**, 463–469.
6. Hsi, C. S., Lu, H. Y. and Yen, F. S., Thermal behaviour of alumina–silica xerogels during calcination. *J. Am. Ceram. Soc.* 1989, **72**(11), 2208–2210.
7. Komarneni, S., Suwa, Y. and Roy, R., Application of compositionally diphasic xerogels for enhanced densification: the system Al_2O_3–SiO_2. *J. Am. Ceram. Soc.* 1986, **69**(7), C155–C156.
8. Wei, W. C. and Halloran, J. W., Phase transformation of diphasic aluminosilicate gels. *J. Am. Ceram. Soc.* 1988, **71**(3), 166–172.
9. Hyatt, M. J. and Bansal, N. P., Phase transformations in xerogels of mullite composition. *J. Mater. Sci.* 1990, **25**, 2815–2821.
10. Lee, J. S. and Yu, S. C., A characterisation of mullite prepared from coprecipitated $3Al_2O_3$–$2SiO_2$ powder. *J. Mater. Sci.* 1992, **27**, 5203–5208.
11. Okada, K. and Otsuka, N., Characterisation of the spinel phase from SiO_2–Al_2O_3 xerogels and the formation process of mullite. *J. Am. Ceram. Soc.* 1986, **69**(9), 652–656.
12. Jin, X. H., Gao, L. and Guo, J. K., The structural change of diphasic mullite gel studied by XRD and IR spectrum analysis. *J. Eur. Ceram. Soc.* 2002, **22**, 1307–1311.
13. Schneider, H., Voll, D., Saruhan, B., Schmucker, M., Schaller, T. and Sebald, A., Constitution of the γ-alumina phase in chemically produced mullite precursors. *J. Eur. Ceram. Soc.* 1994, **13**, 441–448.
14. Low, I. M. and McPherson, R., The origins of the mullite formation. *J. Mater. Sci.* 1989, **24**, 926–936.
15. Chakravorty, A. K., Intermediate Si–Al spinel phase formation in phase transformation of diphasic mullite gel. *J. Mater. Sci.* 1993, **28**, 3839–3844.
16. Srikrishna, K., Tomas, G., Martinez, R., Corral, M. P., De Aza, S. and Moya, J. S., Kaolinite-mullite reaction series; a TEM study. *J. Mater. Sci.* 1990, **25**, 607–612.
17. Li, D. X. and Thomson, W., Mullite formation kinetics of a single-phase gel. *J. Am. Ceram. Soc.* 1990, **73**, 964–969.
18. Gualtieri, A., Bellotto, M., Artioli, G. and Clark, S. M., Kinetic study of the kaolinite-mullite reaction sequence. 2. Mullite formation. *Phys. Chem. Miner.* 1995, **22**, 215–222.
19. Li, D. X. and Thomson, W. J., Kinetics mechanism for mullite formation from sol–gel precursors. *J. Mater. Res.* 1990, **5**, 1963–1969.
20. Lee, J. S. and Yu, S. C., Mullite formation kinetics of coprecipitated Al_2O_3–SiO_2, gels. *Mater. Res. Bull.* 1992, **27**, 405–416.
21. Boccaccini, A. R., Khalil, T. K. and Bucker, M., Activation energy for the mullitization of a diphasic gel obtained from fumed silica and boemite sol. *Mater. Lett.* 1999, **38**, 116–120.
22. Okada, K., Kaneda, J., Kameshima, Y., Yasumori, A. and Takei, T., Crystallization kinetics of mullite from polymeric Al_2O_3–SiO_2 xerogels. *Matt. Lett.* 2003, **57**, 3155–3159.
23. Tkalcec, E., Ivankovic, H., Nass, R. and Schmidt, H., Crystallization kinetics of mullite formation in diphasic gels containing different alumina components. *J. Eur. Ceram. Soc.* 2003, **23**, 1465–1475.
24. Li, D. X. and Thomson, W. J., Mullite formation from non-stoichiometric diphasic precursors. *J. Am. Ceram. Soc.* 1991, **74**, 2382–2387.
25. Huling, J. C. and Messing, G. L., Epitactic nucleation of spinel in aluminosilicate gels and its effect on mullite crystallization. *J. Am. Ceram. Soc.* 1991, **74**, 2374–2381.
26. Takei, T., Kameshima, Y., Yasumori, A. and Okada, K., Crystallization kinetics of mullite in alumina–silica glass fibres. *J. Am. Ceram. Soc.* 1999, **82**, 2876–2880.
27. Takei, T., Kameshima, Y., Yasumori, A. and Okada, K., Crystallization kinetics of mullite from Al_2O_3–SiO_2 glasses under non-isothermal conditions. *J. Eur. Ceram. Soc.* 2001, **21**, 2487–2493.
28. Johnson, B. R., Kriven, W. M. and Schneider, J., Crystal structure development during devitrification of quenched mullite. *J. Eur. Ceram. Soc.* 2001, **21**, 2541–2562.
29. Tkalcec, E., Nass, R., Schmauch, J., Schmidt, H., Kurajica, S., Bezjak, A. *et al.*, Crystallization kinetics of mullite from single-phase gel determined by isothermal differential scanning calorimetry. *J. Non-Cryst. Solids* 1998, **223**, 57–72.
30. Simpson, T. W., Wen, Q., Yu, N. and Clarke, D. R., Kinetics of amorphous $\gamma \rightarrow \alpha$ transformation in aluminium oxide: effect of crystallographic orientation. *J. Am. Ceram. Soc.* 1998, **81**(1), 61–66.
31. Steiner, C. J. P., Hasselman, D. P. H. and Spriggs, R. P., Kinetics of the gamma-to-alpha alumina phase transformation. *J. Am. Ceram. Soc.* 1971, **54**(8), 412–413.
32. Young, R. A., *The Rietveld Method*, ed. International Union of Crystallography. Oxford University Press, 1993.
33. Ban, T. and Okada, K., Structure refinement of mullite by the Rietveld method and a new method for estimation of chemical composition. *J. Am. Ceram. Soc.* 1992, **75**, 227–230.
34. *Bruker Advanced X-ray Solutions*. TOPAS2, 2001.
35. Kissinger, H. E., Variation of peak temperature with heating rate in differential thermal analysis. *J. Nat. Bur. Stand.* 1956, **57**(4), 217–221.
36. Augis, J. A. and Bennet, J. B., Calculation of the Avrami parameters for heterogeneous solid state reaction using a modification of the Kissinger method. *J. Therm. Anal.* 1978, **13**, 283.
37. Kurajica, S., Bezjak, A. and Tkalcec, E., Resolution of overlapping peaks and the determination of kinetic parameters for the crystallization of multicomponent system from DTA or DSC curves. 1. Non-isothermal kinetics. *Thermochim. Acta* 1996, **288**, 123–135.
38. Rajendran, S., Rossell, H. J. and Sanders, J. V., Crystallization of coprecipitated mullite precursor during heat treatment. *J. Mater. Sci.* 1990, **25**, 4462–4471.

39. Schneider, H., Merwin, L. and Sebald, A., Mullite formation from non-crystalline precursors. *J. Mater. Sci*. 1992, **27**, 805–812.
40. Yoldas, B. E., Effect of ultrastructure on crystallization on mullite. *J. Mater. Sci.* 1992, **27**, 6667–6672.
41. Schneider, H., Saruhan, B., Voll, D., Merwin, L. and Sebald, A., Mullite precursor phases. *J. Eur. Ceram. Soc.* 1993, **11**, 87–94.
42. Sueyoshi, S. S. and Soto, C. A. C., Fine pure mullite powder by homogeneous precipitation. *J. Eur. Ceram. Soc*. 1998, **18**, 1145–1152.
43. Kanka, B. and Schneider, H., Sintering mechanisms and microstructural development of coprecipitated mullite. *J. Mater. Sci*. 1994, **29**, 1239–1249.